First principles multielectron mixed quantum/classical simulations in the condensed phase. I. An efficient Fourier-grid method for solving the many-electron problem

William J. Glover, Ross E. Larsen, and Benjamin J. Schwartz[a)]
Department of Chemistry and Biochemistry, University of California, Los Angeles, Los Angeles, California 90095-1569, USA

(Received 19 November 2009; accepted 11 February 2010; published online 8 April 2010)

We introduce an efficient multielectron first-principles based electronic structure method, the two-electron Fourier-grid (2EFG) approach, that is particularly suited for use in mixed quantum/classical simulations of condensed-phase systems. The 2EFG method directly solves for the six-dimensional wave function of a two-electron Hamiltonian in a Fourier-grid representation such that the effects of electron correlation and exchange are treated exactly for both the ground and excited states. Due to the simplicity of a Fourier-grid representation, the 2EFG is readily parallelizable and we discuss its computational implementation in a distributed-memory parallel environment. We show our method is highly efficient, being able to find two-electron wave functions in ~20 s on a modern desktop computer for a calculation this is equivalent to full configuration interaction (FCI) in a basis of 17 million Slater determinants. We benchmark the accuracy of the 2EFG by applying it to two electronic structure test problems: the harmonium atom and the sodium dimer. We find that even with a modest grid basis size, our method converges to the analytically exact solutions of harmonium in both the weakly and strongly correlated electron regimes. Our method also reproduces the low-lying potential energy curves of the sodium dimer to a similar level of accuracy as a valence CI calculation, thus demonstrating its applicability to molecular systems. In the following paper [W. J. Glover, R. E. Larsen, and B. J. Schwartz, J. Chem. Phys. **132**, 144102 (2010)], we use the 2EFG method to explore the nature of the electronic states that comprise the charge-transfer-to-solvent absorption band of sodium anions in liquid tetrahydrofuran. © *2010 American Institute of Physics*. [doi:10.1063/1.3352564]

I. INTRODUCTION

The simulation of electronically excited reactions in the condensed phase from first principles remains a challenge. This is in part because *ab initio* electronic structure methods capable of describing excited states are currently far too costly to be applied directly to the large number of atoms that make up a condensed-phase simulation. The vast majority of computer simulations of electronically excited condensed-phase reactions have therefore used either single-electron model Hamiltonians[1–3] or semiempirical quantum chemical methods.[4–7] Although the low computational cost of such methods favors their use in condensed-phase simulation, a first-principles description of electronic structure would be desirable, particularly for systems where physical insight is lacking or where parametrization to experimental data is not possible.

In this paper, we present a new first-principles electronic structure method that is particularly suited to condensed-phase simulation: the two-electron Fourier-grid (2EFG) method. The method performs a direct diagonalization of a many-electron Hamiltonian in a grid basis set such that it is equivalent to configuration interaction with single and double (CISD) excitations. The basis set is flexible enough to describe both strongly and weakly correlated systems, and because it is a grid, it is readily transferrable from one system to another. As our method is equivalent to CISD, exchange and correlation are treated at a high level (exactly for 2-electron systems) and the excited states are meaningful. Moreover, the method is efficient enough to be performed repeatedly, for example, at each time step of a long molecular dynamics simulation trajectory.

One of the keys to implementing our method in condensed-phase simulations is the use of a mixed quantum/classical (MQC) scheme, which for our purposes entails a quantum mechanical treatment of the valence electrons of a solute molecule and a classical treatment of the solute core and solvent molecules. The classical particles and quantum electrons are coupled through molecular pseudopotentials that are rigorously derived from first-principles quantum chemistry calculations and therefore include Pauli repulsion and exchange interactions in addition to electrostatic interactions between the valence electrons and solvent molecules.[8,9]

In what is presented below, we outline and apply our 2EFG method for two-electron systems. This is because with the use of molecular pseudopotentials,[8,9] many condensed-phase problems of interest are reduced to effective two-electron systems,[10–13] for which our 2EFG method provides an *exact* treatment. (We note that the generalization of our

a)Author to whom correspondence should be addressed. Electronic mail: schwartz@chem.ucla.edu.

2EFG method to additional electrons is straightforward if there are sufficient computational resources). For two-electron systems, our method is efficient enough to be used iteratively in molecular dynamics simulations—even with $\geq 10^8$ basis functions. Thus, the purpose of this paper is to present the development and implementation of our 2EFG method, and to benchmark the accuracy of the method on two test electronic structure problems: the harmonium atom and the sodium dimer. Although our grid-based method is ultimately designed for use in condensed-phase simulation, we chose these gas-phase two-electron problems as they have exact or numerically accurate solutions with which to compare.

In the following paper, hereafter called Paper II,[13] we apply our 2EFG method to the problem of charge-transfer-to-solvent (CTTS) reactions, providing new insight into the excited-state electronic structure of the sodium anion (sodide) in liquid tetrahydrofuran (THF).[14–26] CTTS reactions represent a challenge to simulate from first principles because they involve a valence electron being promoted from an anionic solute to a solvent-supported excited state that ultimately detaches and forms a solvated electron.[14,27–30] The quantum mechanical region for a CTTS reaction thus encompasses not only the solute but also all the solvent molecules that support the CTTS excited state and the detached solvated electron. The fact that our 2EFG method uses a grid representation of the wave function allows it to describe such electronic states that span multiple solvent molecules as well as the spaces between solvent molecules.

The remainder of this paper is outlined as follows. In Sec. II we develop our 2EFG method and discuss its computational implementation. In Sec. III we demonstrate that our 2EFG method can yield numerically exact results by applying it to the harmonium atom. As a test of our method on a molecular system, in Sec. III we also apply our 2EFG method to calculate the electronic states of a gas-phase sodium dimer. We then conclude in Sec. IV, and also present an appendix in which we include details of additional numerical techniques that we used to improve the accuracy and efficiency of the method. Finally, in the supporting information,[31] we show how the 2EFG method improves upon a real-space CISD method that we developed in previous work.[10]

II. DEVELOPMENT OF THE 2EFG METHOD FOR MOLECULAR SIMULATION

A. The advantage of Fourier grids for solving the Schrödinger equation

To introduce our 2EFG method, we start by writing the time-independent Schrödinger equation (TISE) for two electrons in atomic units:

$$\hat{H}|\Psi\rangle = (\hat{h}_1 + \hat{h}_2 + \hat{r}_{12}^{-1})|\Psi\rangle = E|\Psi\rangle, \tag{1}$$

where $\hat{H}$ is the two-electron Hamiltonian, $\hat{h}_i = \hat{T}_i + \hat{V}_i$ is the single-electron Hamiltonian for electron i with kinetic and potential energy operators $\hat{T}_i$ and $\hat{V}_i$, respectively, $\hat{r}_{12}^{-1}$ is the electron-electron Coulomb operator, and $|\Psi\rangle$ is a two-electron eigenstate. To solve Eq. (1), we first express the two-electron eigenstate in a basis of N^6 real-space grid points, which we write in Hilbert space as:

$$|\Psi\rangle = \sum_{i,j}^{N^6} \Psi_{i,j} |\boldsymbol{r}_i \boldsymbol{r}_j\rangle, \tag{2}$$

where $\{|\boldsymbol{r}_i \boldsymbol{r}_j\rangle\}$ is a six-dimensional (6D) grid point basis, $\{\Psi_{i,j}\}$ are real-valued expansion coefficients in this basis, and N is the number of grid points along a single spatial dimension. As indicated by our choice of symbol, $\Psi_{i,j}$ has the physical interpretation of representing the value of the electronic wave function at the 6D real-space coordinate $(\boldsymbol{r}_i, \boldsymbol{r}_j)$ and thus fully describes the spatial properties of both electrons, including their correlation. In other words, Eq. (2) is equivalent to a full CI expansion of the two-electron wave function. We enforce exchange symmetry in our expansion by choosing $\Psi_{i,j} = \pm \Psi_{j,i}$ in the values of the expansion coefficients, with the + and − signs corresponding to singlet and triplet states, respectively; this guarantees that the spatial wave function for a singlet(triplet) state is (anti)symmetric with respect to exchange of electron 1 and 2's coordinates.

In the basis of Eq. (2), the matrix representation of the two-electron Hamiltonian in Eq. (1) has a size of $N^6 \times N^6$, which even for the relatively modest choice of $N=16$ would require 2 petabytes of memory to store the $\sim 3 \times 10^{14}$ matrix elements. Thus, direct diagonalization of this matrix is simply not computationally feasible. Instead, we iteratively solve Eq. (1) for the low-lying states of interest using the Lanczos algorithm,[32] since this approach requires only the multiplication of the Hamiltonian matrix into a vector, which can be performed so that storage scales linearly with the number of basis functions ($\mathcal{O}(N^6)$). To apply the Lanczos algorithm, we take advantage of the fact that in a grid basis, the operation of the Hamiltonian on a wave function can be made particularly simple: the kinetic energy operators are local (have a diagonal matrix representation) in reciprocal space and the potential energy operators are local in real space. Thus, we can use fast Fourier transforms (FFTs) to transform the wave function between real and reciprocal space:

$$\langle \boldsymbol{k}_l \boldsymbol{k}_m | \Psi \rangle \equiv \tilde{\Psi}_{l,m} = \sum_{i,j} F_{i,l} F_{j,m} \Psi_{i,j}, \tag{3}$$

where $\{|\boldsymbol{k}_l \boldsymbol{k}_m\rangle\}$ is a 6D reciprocal-space grid-point basis state, $\boldsymbol{k}_l$ is a dimensionless reciprocal-space vector that has components with integer values running from $-N/2+1$ to $N/2$, $\hat{F}$ is the matrix representation of a three-dimensional FFT with components $F_{i,l}$ and $\tilde{\Psi}_{l,m}$ is the reciprocal-space representation of the wave function. Thus, in atomic units, the operation of the single-electron Hamiltonians, $\hat{h}_1$ and $\hat{h}_2$, on a wave function is:[1]

$$\langle \boldsymbol{r}_i \boldsymbol{r}_j | \hat{h}_1 | \Psi \rangle = ((\hat{F}^{-1} \cdot \hat{T} \cdot \hat{F})_1 \otimes \hat{I}_2 \cdot \Psi)_{i,j} + V(\boldsymbol{r}_i) \Psi_{i,j}, \tag{4}$$

$$\langle \boldsymbol{r}_i \boldsymbol{r}_j | \hat{h}_2 | \Psi \rangle = (\hat{I}_1 \otimes (\hat{F}^{-1} \cdot \hat{T} \cdot \hat{F})_2 \cdot \Psi)_{i,j} + V(\boldsymbol{r}_j) \Psi_{i,j}, \tag{5}$$

where $\hat{T}$ is the kinetic energy operator, which is diagonal in reciprocal space with matrix elements

$$\tilde{T}_{l,l} = (2\pi/L)^2 \boldsymbol{k}_l^2/2, \tag{6}$$

where L is the length of the grid in one dimension, $V(\boldsymbol{r}_i)$ is the real-space representation of the potential energy operator at grid point location $(\boldsymbol{r}_i)$, and $\hat{I}$ is the identity matrix. The subscripts 1 and 2 in Eqs. (4) and (5) indicate which of the two electrons the operator acts on. Thus, the first term of Eq. (4), which applies the kinetic energy operator to the real-space representation of the two-electron wave function, can be read as: leaving electron 2's wave function alone, FFT the wave function coordinates of electron 1, multiply by the diagonal kinetic energy matrix, and then inverse FFT electron 1's wave function. Equations (4)–(6) reveal two reasons why Fourier-grid methods are particularly efficient. First, the elements of the kinetic energy operator never change, so they need only be calculated once and tabulated for use in molecular simulation. Second, due to the scaling of the FFT, the computational cost of solving Eq. (4) scales only as N^6 Log N, which is close to linear scaling in the size of the basis. In our 2EFG implementation, we use a slightly modified version of Eqs. (4) and (5) that corrects aliasing errors in the FFT, as described in more detail in Sec. 1 of the Appendix.

In addition to the fact that the kinetic energy operator has a diagonal representation in reciprocal space, a Fourier-grid representation of the wave function provides the advantage that the electron-electron Coulomb operator, $\hat{r}_{12}^{-1}$, also has a diagonal representation in the 6D real-space basis of Eq. (2). This feature stands in stark contrast to approaches based on Gaussian basis functions, where $\hat{r}_{12}^{-1}$ has a dense-matrix representation whose calculation, storage and use are the most computationally demanding parts of traditional quantum chemistry calculations.[33] Although the Fourier-grid representation of the electron-electron interaction is diagonal, there is an issue of the divergence in $\hat{r}_{12}^{-1}$ at $\boldsymbol{r}_1 = \boldsymbol{r}_2$, since this singularity cannot be represented on a finite real-space grid. We deal with this singularity following an approach we previously developed for evaluating two-electron integrals on a real-space grid that takes the wave function to be piece-wise constant.[10] With this assumption, the matrix elements of the electron-electron Coulomb operator in the 6D real-space grid basis become:

$$\langle \boldsymbol{r}_i \boldsymbol{r}_j | \hat{r}_{12}^{-1} | \boldsymbol{r}_k \boldsymbol{r}_l \rangle = a^{-1} \phi_{i,j} \delta_{i,k} \delta_{j,l}, \tag{7}$$

where a is the grid-spacing, δ is a Kronecker delta and

$$\phi_{i,j} = \int_0 d^3\boldsymbol{r} \int_{|i-j|} d^3\boldsymbol{r}' \frac{1}{|\boldsymbol{r} - \boldsymbol{r}'|} \tag{8}$$

is the Coulomb interaction between two uniformly charged unit cubes, one located at the origin and the other located at $(\boldsymbol{r}_i - \boldsymbol{r}_j)/a$ (that is, at grid point "$i-j$"). By writing Eq. (8) in terms of unit cubes, $\phi_{i,j}$ does not depend on the grid spacing, and thus it only needs to be evaluated once and tabulated for future use. As in our previous work,[10] we evaluated Eq. (8) using the numerical integration routines in Mathematica for each of the $N(N+1)(N+2)/6$ pairs of cubes that have distinct values of $\phi_{i,j}$, and we set $\phi_{i,j} = a/(|\boldsymbol{r}_i - \boldsymbol{r}_j|)$ for cube displacements greater than 16 grid points. Although a piece-wise constant quadrature is a low-order approximation, we showed previously that it yields electron-electron Coulomb matrix elements between particle-in-box (PIB) eigenstates that rapidly converge to the exact results with increasing grid density.[10] Thus, we expect that application of our 2EFG method to any two-electron problem will yield essentially exact results, providing the real-space grid is dense enough. We shall explore the convergence of our method in chemically relevant systems below in Sec. III.

Using the piece-wise constant quadrature of Eq. (7), the operation of the electron-electron Coulomb operator on a wave function is:

$$\langle \boldsymbol{r}_i \boldsymbol{r}_j | \hat{r}_{12}^{-1} | \Psi \rangle = a^{-1} \Psi_{i,j} \phi_{i,j}. \tag{9}$$

The operation of the full Hamiltonian on a wave function is thus obtained by adding the results of Eqs. (4), (5), and (9) which, when used as input to the Lanczos algorithm,[32] allows us to iteratively solve Eq. (1) for the electronic states of interest.

B. Comparison to other grid-based many-electron wave function methods

It is worth noting that other grid-based many-electron wave function methods have been presented in the literature. For example, Alavi used PIB states to study the properties of two interacting electrons in a box.[34] Although his method used an efficient mixed real and reciprocal-space grid quadrature to evaluate the electron-electron integrals in the PIB basis, the Hamiltonian had a dense matrix representation and therefore would be too costly to implement for condensed-phase systems that require a large basis expansion. In addition, we previously developed a real-space CI method[10] and used it to study the hydrated dielectron[35–37] and aqueous sodide.[11] As shown in the Supporting Information,[31] our 2EFG method is related to our previous real-space CI method. Our previous method, however, was limited to only a few tens of basis functions. This means that for many systems, the lack of a complete basis leads to poor energy conservation when calculating the forces on the classical particles from the quantum mechanical electrons, so that costly Pulay force corrections[38] would be necessary for rigorous energy conservation. This problem is avoided in our 2EFG method, which variationally optimizes wave functions in a stationary basis at every time step. Finally, Kubota and Nobusada developed a discrete variable representation (DVR) method to study exciton states (electron-hole wave functions) in quantum boxes.[39,40] Due to the similarities of DVR and Fourier grid representations,[41] Kubota and Nobusada's approach is also related to our 2EFG method, although it is appropriate only for calculating spinless exciton states.

C. Computational implementation of the 2EFG

Having presented the foundation of our CI-based 2EFG method, we now discuss the details of its computational implementation. Since our goal is to use the 2EFG method repeatedly, at each time step of a MQC molecular dynamics

(MD) simulation, in this section we also highlight the steps we took to make the 2EFG method as efficient as possible.

There are two principal factors that determine the computational cost of our 2EFG method. The first is how many iterations the Lanczos algorithm takes to converge to the desired eigenvalues when solving Eq. (1). We reduced the number of iterations by using a Chebychev spectral transform, as outlined in Sec. 2 of the Appendix. The second computational cost in our method is associated with the storage and manipulation of large 6D wave functions. Even for systems that remain localized in a small region of space so that the wave function can be adequately described by a modest grid basis, e.g., $N=16$, each 6D wave function is represented by 16^6 numbers, which requires roughly 128 Mbyte of storage. Although this is well within the limits of modern desktop computers, for larger systems, we find that bases of up to $N=32$ are necessary, requiring 32^6 numbers or roughly 8 Gbyte of storage per wave function. To store and manipulate wave functions of this size, we use distributed-memory parallel processing and split the wave functions, $\Psi_{i,j}$ in the j index among n_{CPU} CPUs. Communication between CPUs is handled with the message passing interface (MPI).[42] We make use of a parallel implementation of the implicitly restarted Lanczos method (IRLM)[43] called PARPACK that also relies on MPI.[44]

To simplify the operation of the Hamiltonian and to reduce the amount of communication needed between the CPUs, we note that the operation of $\hat{h}_2$ in Eq. (1) is related to $\hat{h}_1$ by permutation symmetry:

$$\hat{h}_2|\Psi\rangle = \pm \hat{P}_{12}\hat{h}_1|\Psi\rangle, \tag{10}$$

where the +(−)-sign is for singlet(triplet) states and $\hat{P}_{12}$ permutes the coordinates of electrons 1 and 2.[45] Using Eq. (10), and noting that $\hat{r}_{12}^{-1}$ remains unchanged upon permutation of the electrons' coordinates, the operation of the full two-electron Hamiltonian becomes:

$$\hat{H}|\Psi\rangle = \left(\frac{\hat{I} \pm \hat{P}_{12}}{2}\right)(2\hat{h}_1 + \hat{r}_{12}^{-1})|\Psi\rangle, \tag{11}$$

where $\hat{I}$ is the identity operator and the +(−)-sign is for singlet(triplet) states. The advantage of Eq. (11) is that the operation of $\hat{h}_1$ and $\hat{r}_{12}^{-1}$ is local to each CPU and therefore no communication between CPUs is necessary for these terms. The $\hat{P}_{12}$ operator swaps the indices of the wave function expansion vector: $\hat{P}_{12}\Psi_{i,j}=\Psi_{j,i}$. This transpose necessarily involves communication between the CPUs, but it can be accomplished easily using an MPI all-to-all communication routine.

An added bonus of using Eq. (11) is that $(\hat{I}\pm\hat{P}_{12})/2$ projects out wave function components of any unwanted spin symmetry. For example, operating $(\hat{I}+\hat{P}_{12})/2$ on a mixed spin state removes the triplet component of the wave function but leaves the singlet component untouched. Although the Hamiltonian in Eq. (1) is spin invariant and there should be no formal mixing of spin states, numerical round-off error will gradually cause spin mixing after repeated operation of the Hamiltonian on an expansion vector. The use of Eq. (11) removes this error at no additional computational cost.

III. TESTING THE 2EFG METHOD

Having presented all of the elements of our 2EFG method, in this section we demonstrate its applicability to chemically relevant two-electron systems. For this purpose, we have tested our 2EFG method on two well-studied two-electron systems: harmonium, which is a model atom consisting of two electrons in a harmonic well potential, and the sodium dimer molecule, Na_2. We chose these problems as they have exact or numerically accurate solutions with which to compare. Furthermore, they represent a rigorous test of our cubic-grid-based method on problems with noncubic symmetry.

A. Harmonium

The Hamiltonian for the two electrons of harmonium in atomic units is:

$$\hat{H} = -\frac{1}{2}\nabla_1^2 - \frac{1}{2}\nabla_2^2 + \frac{1}{2}\omega^2\boldsymbol{r}_1^2 + \frac{1}{2}\omega^2\boldsymbol{r}_2^2 + r_{12}^{-1}, \tag{12}$$

where ω is the harmonic oscillator frequency. Harmonium has received considerable attention as a model by which to test density functionals.[46–53] This is because Eq. (12) becomes separable with a change in coordinates so that the TISE has analytic solutions for a particular, infinite set of ω, the three largest of which are $\omega=0.5$, 0.1 and 0.036 537 3 atomic units.[54] The largest two values of ω yield weakly correlated electrons while all of the others ($\omega=0.036\ 537\ 3$ and smaller) give strongly correlated electrons.[55] Thus we can test our method on harmonium in both weakly and strongly correlated electron regimes, and compare the results from our method to the exact answer.

To test our 2EFG method, we chose two oscillator frequencies: $\omega=0.5$ and 0.036 537 3. For each of these two values of ω we first adjusted the length of the simulation cell (by adding grid points while keeping the grid-spacing fixed at 0.375 Å for $\omega=0.5$ and 1.4375 Å for $\omega=0.036\ 537\ 3$) until the ground-state energy was converged to within one part in 10^5; for $\omega=0.5$, this was found to be 6 Å. For $\omega=0.036\ 537\ 3$ a larger simulation length of 23 Å was required because the confining potential is much shallower than for $\omega=0.5$, so the ground-state wave function is much more diffuse. For these two oscillator frequencies, the lowest eigenvector was found using the IRLM[43] as coded in PARPACK.[44] We used the dealiasing procedure, described in Sec. 1 of the Appendix, with $N_d=2N$. Since the Harmonium calculations were not particularly computationally intensive, we did not use the Chebychev polynomial transform described in Sec. 2 of the Appendix.

After having found the appropriate simulation box lengths for the two values of ω, we then explored the convergence of the ground-state energy with the grid density, as summarized in Table I. We see that an accuracy of ~0.1% in the ground-state energy can be achieved even with a fairly modest number of grid points ($N=20$) in both the weakly and strongly correlated regimes. Furthermore, we also see that on

TABLE I. Convergence properties of the ground-state energy (in atomic units) of harmonium for two oscillator frequencies, ω, calculated via our 2EFG method with different grid densities and comparison to the exact results.

N [a]	$E(\omega=0.5)$ [b]	$E(\omega=0.036\ 537\ 3)$ [c]
12	1.9930	0.219 085
16	1.9964	0.219 168
20	1.9978	0.219 195
24	1.9986	0.219 206
28	1.9990	0.219 212
32	1.9992	0.219 215
Exact	2.0	0.219 224

[a]The number of wave function grid points per dimension. Dealiasing was used with $N_d=2N$.
[b]For this set of calculations, the simulation grid spanned 6 Å on a side.
[c]For this set of calculations, the simulation grid spanned 23 Å on a side.

increasing the grid density, the ground-state energies rapidly converge to the exact solutions. We are thus encouraged that our 2EFG method, despite representing the electronic wave function on a cubic grid, is able to accurately treat a system with spherical symmetry.

To explore the quality of the solutions with our method in more detail we also considered several properties of the ground-state wave functions. Since a 6D wave function is not easily visualized, we instead considered two different densities: the electron density,

$$\rho(\boldsymbol{r}) = 2\int |\Psi(\boldsymbol{r},\boldsymbol{r}_2)|^2 \mathrm{d}\boldsymbol{r}_2, \tag{13}$$

and the intracular density,

$$I(\boldsymbol{r}) = \int\int |\Psi(\boldsymbol{r}_1,\boldsymbol{r}_2)|^2 \delta(\boldsymbol{r}-\boldsymbol{r}_1+\boldsymbol{r}_2)\mathrm{d}\boldsymbol{r}_1\mathrm{d}\boldsymbol{r}_2. \tag{14}$$

The intracular density gives the probability of finding the electrons with a certain displacement from each other; i.e., $I(\boldsymbol{r})$ characterizes the two electrons' spatial correlation. Due to the spherical symmetry in the harmonium Hamiltonian, both the ground-state electron density and intracular density are defined by radial functions. The topological features of $\rho(r)$ and $I(r)$ and how they relate to the degree of electron correlation in harmonium have been discussed in detail elsewhere,[55] so we will not repeat them here except to discuss how our 2EFG method compares with exact results.

The green × symbols in Fig. 1 show $\rho(r)$ for $\omega=0.5$ [panel (a)] and $\omega=0.036\ 537\ 3$ [panel (b)] as calculated with our 2EFG method with $N=32$. The exact radial electron density, plotted as the solid black curve in each panel, has a maximum at $r=0$ for $\omega=0.5$, but the maximum is shifted off the origin to $r\approx 1.3$ bohr for $\omega=0.036\ 537\ 3$. The presence of the maximum at $r>0$ for $\omega=0.036\ 537\ 3$ is indicative of the strongly correlated regime: the electrons are repelling each other strongly enough relative to the harmonic confining potential that the electron density no longer peaks at the harmonic well minimum. For both $\omega=0.5$ and $\omega=0.036\ 537\ 3$, we see that the 2EFG method produces densities that are in excellent agreement with the exact results. In panel (b)'s inset, the region around $r=0$ is expanded to show that the 2EFG method also correctly captures the maximum in $\rho(r)$ at $r\approx 1.3$ bohr, although the 2EFG density is slightly overestimated in this region. We found that the ground-state electron density of harmonium calculated with

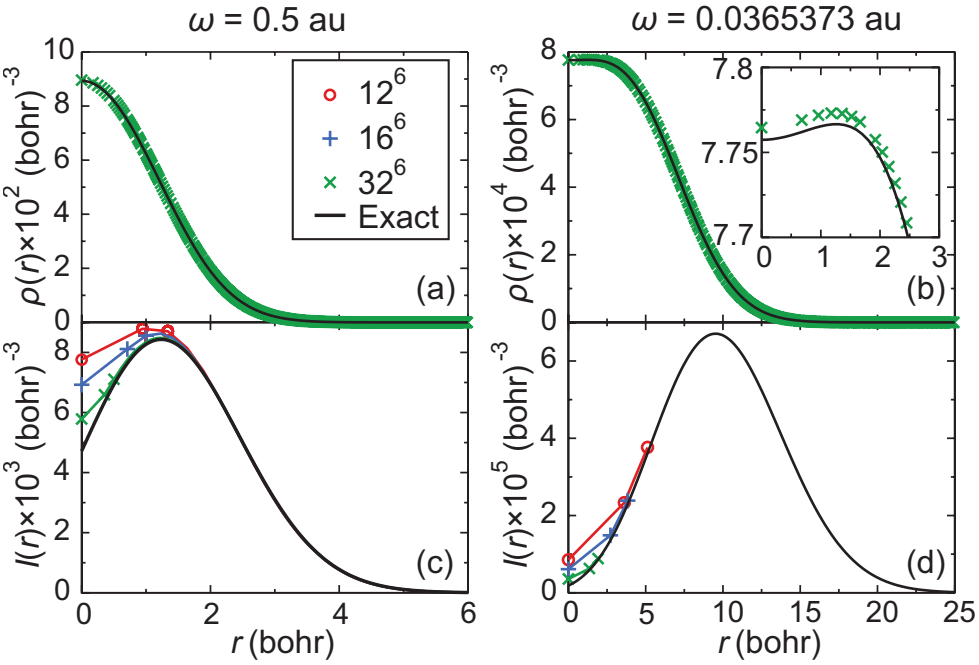

FIG. 1. Properties of the electronic ground state of harmonium. Panels (a) and (b): radial electron density, $\rho(r)$, for $\omega=0.5$ a.u. and $\omega=0.036\ 537\ 3$ a.u., respectively. Panels (c) and (d): intracular density, $I(r)$, for $\omega=0.5$ a.u. and $\omega=0.036\ 537\ 3$ a.u., respectively. The exact results are plotted as the solid black curves and the numerical 2EFG results for different grid densities are plotted as symbols at the grid point locations (red ∘: $N=12$, blue +: $N=16$, and green ×: $N=32$). Only the $N=32$ results are shown in panels (a) and (b). The inset in panel (b) expands the region around $r=0$. For clarity, in panels (c) and (d), we plot $I(r)$ only for the three grid points closest to the origin and connect them with lines to guide the eye.

smaller grid-basis sizes of $N=12$ and $N=16$ (not shown for clarity) are also in excellent agreement with the exact results.

The colored symbols in Figs. 1(c) and 1(d) show the intracular density, $I(r)$ calculated from our 2EFG method for $\omega=0.5$ and $\omega=0.036\,537\,3$, respectively; the different symbols show the results for different grid densities. The exact intracular density is plotted as the solid black curve in each panel. For both $\omega=0.5$ and $\omega=0.036\,537\,3$ we see that the 2EFG results are in excellent agreement with the exact results for r greater than the maximum in $I(r)$ (at $r\approx 1.25$ bohr for $\omega=0.5$ and at $r\approx 9.5$ bohr for $\omega=0.036\,537\,3$), even for the calculation with the fewest grid points, $N=12$ (red circles). For values of r around the minimum and smaller, the agreement is not as good, with the 2EFG calculation tending to overestimate the intracular density in the small r region. But as expected, the 2EFG intracular densities rapidly converge on the exact results as the grid density increases.

It is perhaps not surprising that the greatest error in the 6D 2EFG wave function, $\Psi(\boldsymbol{r}_1,\boldsymbol{r}_2)$, occurs in regions of space where $\boldsymbol{r}_1$ is close to or equal to $\boldsymbol{r}_2$ since this is where the piece-wise constant approximation to the Coulomb matrix elements [Eq. (7)] is most severe. Our approximation that the electron-electron repulsion is averaged over a cube around each grid point underestimates the magnitude of the repulsion and thus overestimates the intracular density when the electrons are in the same region of space. Despite the appearance of this discretization error in the calculated intracular densities, we are encouraged by the fact that the discretization appears not to affect the quality of the calculated 2EFG electron density, $\rho(r)$, which is what defines most properties of interest of the system. Also encouraging is that the discretization error can be made negligibly small by increasing the density of grid points as shown by the convergence of $I(r)$ to exact results with increasing N. Given the above, we believe our 2EFG method can be used to model many-electron systems with quantitative accuracy.

B. Molecular test: Potential energy curves of the sodium dimer

As a test of the applicability of our 2EFG method to a molecular system, we consider the potential energy curves (PECs) for the lowest two singlet states ($X\ ^1\Sigma_g^+$ and $A\ ^1\Sigma_u^+$) and the lowest triplet state ($a\ ^3\Sigma_u^+$) of an isolated sodium dimer molecule, Na_2, which in the frozen-core approximation becomes an effective two-electron system.[56] Calculating the electronic states of Na_2 is an interesting test of our 2EFG method due to the importance of electron correlation in this system: Na_2 is unbound at the Hartree–Fock level.[56] Furthermore, as in all diatomic molecules, static electron correlation becomes increasingly important as the molecule is stretched. Although we expect our CI-based method to work well in the dissociation limit, does the piece-wise constant approximation in the electron-electron integrals give smooth PECs? How well does a 6D cartesian grid do for a molecular system with cylindrical symmetry? Unlike the harmonium system, we have no exact solutions of the electronic states of Na_2 with which to compare; however, we can compare our calculated PECs to experimental results[57,58] and to high-level quantum chemical calculations.[59]

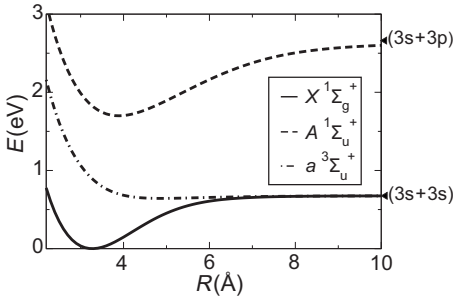

FIG. 2. Gas-phase Born–Oppenheimer PECs of Na_2 calculated with the 2EFG method using $N=28$ for the lowest two singlet [$X\ ^1\Sigma_g^+$ (solid curve) $A\ ^1\Sigma_u^+$ (dashed curve)] and lowest triplet [$a\ ^3\Sigma_u^+$ (dot-dashed curve)]. The dissociation limits are indicated on the right of the figure.

Within the frozen-core approximation, Na_2 is comprised of two classical Na^+ cores and two valence electrons that we treated using our 2EFG method. The electronic wave function of these electrons was expressed on a 6D grid with $N=28$ (and $N_d=48$ in the dealiasing procedure described in Appendix, Sec. 1) that spanned a simulation cell of 21 Å. The length of the simulation cell was chosen to be large enough to avoid artifacts in the PECs from the periodic boundary conditions inherent in the use of the FFTs. The interaction of the electrons and Na^+ cores was treated as a sum of two one-body Philips–Kleinman pseudopotentials centered on each Na^+ core.[11] The classical interaction between the two Na^+ cores was taken to be the Coulombic interaction of two point charges (in other words, we neglected short-range repulsion between the cores at the near-equilibrium internuclear separations of interest). Periodic boundary conditions were not applied to any of the potential energy interactions.

Since the singlet and triplet manifolds arise from different Hamiltonian matrices in our 2EFG formulation [Eq. (11)], the PECs for these manifolds were generated from separate calculations. First we mapped out the Born–Oppenheimer PECs for the lowest two states in the singlet manifold of Na_2 starting from a bond-length of $R=2.2$ Å and reaching $R=10$ Å in increments in 0.1 Å. The dimer was placed in the center of the simulation cell with its internuclear axis along the diagonal to minimize effects of the periodic boundary conditions from the use of FFTs. Starting from a randomly generated wave function, PARPACK was used to iteratively find the lowest two energy eigenvectors in the singlet manifold of Na_2 at $R=2.2$ Å. Eigenvectors at subsequently longer bond-lengths were iteratively found using the eigenvector at the previous bond length as an initial guess. The whole process was then repeated for the lowest state of the triplet manifold. For all the Na_2 calculations, we used a Chebychev polynomial transform with $m=6$ as described in Sec. 2 of the Appendix.

Figure 2 shows the Born–Oppenheimer PECs for the singlet $X\ ^1\Sigma_g^+$ (solid curve) and $A\ ^1\Sigma_u^+$ (dashed curve) states and the $a\ ^3\Sigma_u^+$ (dot-dashed curve) triplet state as a function of the sodium dimer's bond displacement, R. The zero of energy is

TABLE II. Spectroscopic constants for the lowest two singlet states and lowest triplet state of the sodium dimer as calculated with our 2EFG method and obtained from previous calculations and experiment.

State	Method	R_e [a] (Å)	T_e [b] (eV)	ω_e [c] (cm^{-1})	D_e [d] (eV)
$X\ ^1\Sigma_g^+$	2EFG	3.27	0	136	0.676
	Liu *et al.* (Ref. 60)	3.34	0	136	0.458
	Magnier *et al.* (Ref. 59)	3.09	0	159.1	0.731
	Experiment (Ref. 57)	3.08	0	159.2	0.747
$A\ ^1\Sigma_u^+$	2EFG	3.89	1.84	110	0.962
	Magnier *et al.* (Ref. 59)	3.63	1.81	117.5	1.03
	Experiment (Ref. 63)	3.64	1.82	117.3	1.03
$a\ ^3\Sigma_u^+$	2EFG	4.89	0.8919	33.0	0.0330
	Magnier *et al.* (Ref. 59)	5.19	0.7089	23.9	0.0216
	Experiment (Ref. 58)	5.09	0.7251	24.5	0.0216

[a]Equilibrium bond length.
[b]Vertical excitation energy from ground state at equilibrium bond length.
[c]Harmonic frequency at equilibrium bond length.
[d]Dissociation energy.

taken to be the minimum of the $X\ ^1\Sigma_g^+$ PEC. To verify the dissociation limits, we also calculated the electronic energies of two infinitely separated sodium atoms using a one-electron Fourier-grid method. These energies are indicated with arrows on the right of the figure. The overall features of the PECs in Fig. 2 are encouraging: the $X\ ^1\Sigma_g^+$ and $a\ ^3\Sigma_u^+$ states correctly dissociate to $3s+3s$ and the $A\ ^1\Sigma_u^+$ state correctly dissociates to $3s+3p$. Furthermore all the PECs are smooth, despite discretizing the electronic wave function of a cylindrically symmetric system in a cartesian grid basis.

To assess the quality of our method, we also calculated various spectroscopic constants of Na_2 from the 2EFG-generated PECs, which along with the experimental values[57,58] are summarized in Table II. Table II also lists values obtained from the frozen-core pseudopotential +valence CI calculations of Liu, Carter, and Carter,[60] which (although they use Gaussian basis functions instead of a grid basis) are the closest in spirit to our 2EFG method. We note that Liu *et al.* only studied the ground electronic state of Na_2, so for the excited states, we also compare our results in Table II to the quantum chemistry calculations of Magnier *et al.*, whose calculations are expected to be more accurate than ours as they go beyond the frozen-core approximation by including core polarization potentials (CPPs).[59] Finally, we also note that the ground-state dissociation energy calculated by Liu *et al.* is too small, a result that Liu *et al.* ascribe to the small size of the basis set they employed in their calculation.[60]

A quick examination of Table II shows that for the ground-state ($X\ ^1\Sigma_g^+$) PEC, our 2EFG method is in good agreement with experiment: all of the 2EFG-calculated spectroscopic constants are accurate to within ~10%. Our spectroscopic constants also agree with Liu *et al.*'s theoretical results.[60] For the $A\ ^1\Sigma_u^+$ and $a\ ^3\Sigma_u^+$ states, we also find reasonable agreement between our 2EFG results and experiment. The fact that our 2EFG calculation correctly predicts the features of the $A\ ^1\Sigma_u^+$ state shows that we can treat electronic excited states on an equal footing with the ground state, as expected for a CI-based method. We note that the calculations of Magnier *et al.* are in better agreement with experiment than those from our 2EFG method.[59] We do not believe that the larger discrepancy between our results and experiment points to a failing of the 2EFG method; rather, we believe that this is a direct result of the need to include CPPs to obtain quantitative accuracy for the alkali dimers, as argued by Müller and Meyer.[56] Although we could include CPPs in our 2EFG method in principle, it would involve introducing a two-electron core polarization operator [Eq. 5d of Ref. 56] that scales as N_{at}^2, where N_{at} is the number of classical atomic cores in the simulation, thereby limiting the method to small systems. Since our ultimate goal is to apply the 2EFG method to study the dynamics in condensed phases where hundreds of atoms must be simulated, we decided to neglect core polarization. We thus view the 2EFG method with our current choice of potentials as providing a qualitatively (and near-quantitatively) accurate description of the bonding properties of Na_2 that will be sufficient to study its properties in condensed-phase environments, as we have explored elsewhere.[12]

IV. DISCUSSION

In this paper, we presented a new electronic structure method based on a Fourier-grid representation of many-electron wave functions: the 2EFG method. We showed that a Fourier-grid representation, combined with an appropriate grid-based quadrature to evaluate electron-electron repulsion integrals, affords a very sparse matrix representation of two-electron Hamiltonians. This sparseness allowed our method to easily be parallelized and in Sec. 2 of the Appendix, we demonstrate that it takes a modern desktop computer only ~20 s to solve the Schrödinger equation for the lowest state of sodide in liquid THF, a problem that is equivalent to full CI in a basis of 17 million Slater determinants. This speed makes the 2EFG method suitable for use in a MQC molecular dynamics algorithm where the Schrödinger equation must be solved at every molecular dynamics time step, as we demonstrate in Paper II.

Our 2EFG method is not only highly efficient but it is also highly accurate: our benchmark calculations on the har-

monium atom showed that our 2EFG method gives millihartree accuracy in electronic eigenvalues, even for modest grid point basis sizes. We also demonstrated that the 2EFG method can handle molecular systems by calculating the PECs of the sodium dimer to a similar level of accuracy as a full CI calculation that used Gaussian basis functions. However, unlike electronic structure methods based on Gaussian basis functions, our 2EFG method can easily capture electronic wave functions that are localized away from atomic cores, such as the CTTS states of atomic anions,[11] as also demonstrated in detail in Paper II. Although our 2EFG method is both efficient and accurate, we do not claim that it should replace traditional quantum chemistry approaches to gas-phase problems, where the use of localized basis functions is more optimal.

We close by noting that our 2EFG method could easily be adapted to study other correlated quantum particles, for example, positronium, in condensed-phase environments. Another extension would be to treat systems with more than two electrons. A brute force approach of directly applying our Fourier-grid method to systems of more than two electrons would be limited by a computational cost that scales exponentially with the number of electrons. This limitation may be alleviated to some degree by employing an adaptive grid whereby grid points that do not contribute to the wave functions of interest are removed from the calculation thus reducing the size of the Hamiltonian matrix. A promising alternative to the brute force approach would be to use instead a limited number, N_{wf}, of two-electron wave functions to form a set of direct-product basis states in which the many-electron wave function, $|\Phi\rangle$, is expanded (e.g., a four-electron wave function could be written as $|\Gamma\rangle=\Sigma_i^{N_{\mathrm{wf}}}\Sigma_{j>i}^{N_{\mathrm{wf}}}\hat{A}|\Psi_i\rangle|\Psi_j\rangle$, where $\hat{A}$ is the antisymmetrizer and $|\Psi_i\rangle$ is the two-electron state i). Since the electron-electron Coulomb operator would couple direct-products differing by no more than a single two-electron wave function, the many-electron Hamiltonian would have an extremely sparse representation in this truncated direct-product space. Assuming that the construction of the Hamiltonian matrix is the computational bottleneck, the method would scale as $N_{\mathrm{wf}}^2N^6$ *regardless of the number of electrons*. Although the inherent truncation in the wave function means that electron correlation will be treated approximately, we believe such an approach will be sufficiently accurate to study systems of many electrons, while retaining all the benefits of using a Fourier grid to represent the wave function.

ACKNOWLEDGMENTS

This work was supported by the National Science Foundation under Grant Nos. CHE-0603766 and CHE-0908548 and the American Chemical Society Petroleum Research Fund under Grant No. 45988-AC,6. The authors thank Prakashan Korambath, Tajendra Vir Singh, Shao-Ching Huang, Viktor Decyk, and Warren Mori for helpful discussion in the parallelization of our algorithm. We also gratefully acknowledge the UCLA Institute for Digital Research and Education for allocating computer time for the calculations presented in this paper.

APPENDIX: ADDITIONAL IMPLEMENTATION DETAILS IN THE 2EFG METHOD

In this appendix, we discuss how we improved the accuracy and efficiency of our 2EFG method with two standard numerical techniques. The first improvement concerns the removal of aliasing errors from the use of Fourier transforms. The second improvement increases the efficiency of the Lanczos diagonalization in our method with the use of a Chebychev spectral transform.

1. Aliasing errors in Fourier-grid approaches

To understand why aliasing errors can arise in Fourier-grid approaches, we rewrite Eq. (4) in reciprocal space:

$$\langle \boldsymbol{k}_l\boldsymbol{k}_m|\hat{h}_1|\Psi\rangle = (2\pi/L)^2\frac{\boldsymbol{k}_l^2}{2}\tilde{\Psi}_{l,m} + \sum_{l'}\tilde{V}(\boldsymbol{k}_l-\boldsymbol{k}_{l'})\tilde{\Psi}_{l',m}, \tag{A1}$$

where $\tilde{V}(\boldsymbol{k}_l-\boldsymbol{k}_{l'})$ is the reciprocal-space representation of the potential energy operator. In reciprocal space, the potential energy operator is nonlocal and must be represented by $(2N-1)^3$ reciprocal-space vectors (since both $\boldsymbol{k}_l$ and $\boldsymbol{k}_{l'}$ have components that run from $-N/2+1$ to $N/2$). Fourier-grid techniques that use the same number of real-space grid points as k-space vectors to represent the potential energy operator[41] are thus subject to aliasing errors. Of course, we always expect aliasing errors to decrease as the density of the grid increases (the large N limit). However, we wish to keep N as small as possible since the size of the basis in the 2EFG method is N^6.

Our approach to reducing aliasing errors is to store only the single-electron potential energy operator (and not the electron-electron Coulomb operator) on a denser grid of $(2N-1)^3$ grid points. This means that the wave function also must be interpolated from N^3 to $(2N-1)^3$ real-space grid points in electron 1's coordinates when applying the potential energy operator. To achieve this interpolation, we use the standard technique of FFTing the wave function to reciprocal space, padding the reciprocal-space function with m zeros in each dimension and then inverse FFTing to give an interpolated real-space function on a denser grid of $N_d=N+m$ points per dimension. In practice, we need not always interpolate to as many $(2N-1)^3$ real-space grid points as $N^d\approx(3/2)N$ (or smaller) is often sufficient, as determined empirically by convergence checks.

2. Chebyshev polynomial spectral transform

For our 2EFG method to be efficient, we require that the Lanczos diagonalization converge in as few iterations as possible. In general, the convergence properties of Lanczos methods are dictated by the distribution of eigenvalues; convergence is fastest for well-separated eigenvalues at one end of the spectrum.[32] For most problems of interest, we will be calculating only the lowest-lying eigenvalues. So, for optimum efficiency in our 2EFG method, it is desirable that these eigenvalues be well-separated from the rest of the spectrum. In this section, we show how we accomplish this through the use of a spectral transform.

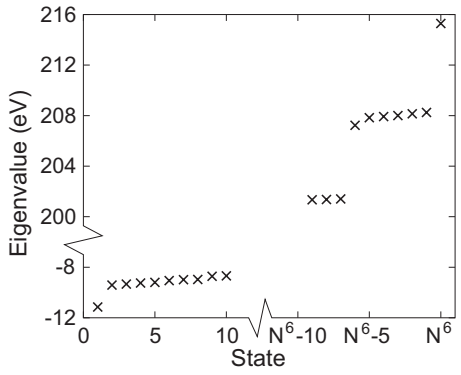

FIG. 3. Distribution of the eigenvalues for sodide in a single liquid THF configuration. Only the ten lowest and highest eigenvalues are calculated so there are breaks in the axes. Details of the simulation are given in Sec. II of Paper II. For this calculation, the number of grid points and hence the number of eigenvalues is $N^6=16^6=16\,777\,216$.

Figure 3 shows the distribution of electronic energy eigenvalues for the two valence electrons of sodide in THF, a system that we explore in more detail in Paper II. The Figure shows that the low-lying eigenvalues of interest are much more closely spaced than the highest eigenvalues, precisely the opposite of the situation we desire for optimum efficiency of the Lanczos method. The figure also shows a pattern in the distribution of the highest eigenvalues: there is a large energy gap between the highest eigenvalue and a cluster of six lower quasidegenerate eigenvalues, followed by another large gap to the next cluster of lower eigenvalues. This pattern matches exactly the distribution of the highest eigenvalues of the kinetic energy operator in a 6D-grid basis: in other words, the high-energy part of the spectrum is dominated by the kinetic energy operator. Since the kinetic energy operator is the same for any two-electron system, we anticipate that the high-energy part of the spectrum from our 2EFG method will have the same features seen in Fig. 3 for any two-electron system. If left unchecked, this could cause problems for the convergence of the IRLM for low-lying eigenstates.

To solve this problem, we have chosen to employ a spectral transform, where instead of diagonalizing $\hat{H}$ directly, we diagonalize a function Θ of $\hat{H}$:[61]

$$\Theta(\hat{H})|\Psi\rangle=\lambda|\Psi\rangle, \tag{A2}$$

where the eigenstates of $\Theta(\hat{H})$ are the same as those of $\hat{H}$, allowing the eigenvalues of $\hat{H}$ to be found from the Rayleigh quotient:

$$E=\langle\Psi|\hat{H}|\Psi\rangle/\langle\Psi|\Psi\rangle. \tag{A3}$$

If the eigenvalues of interest lie in the interval $(E_{\min},E_{\text{cutoff}})$, then Θ is chosen such that the transformed matrix $\Theta(\hat{H})$ has well-separated eigenvalues in the interval of interest, while the eigenvalues in regions outside those of interest are compressed.

One of the most commonly used spectral transforms is the shift-and-invert (SI) function, $\Theta^{\text{SI}}(\hat{H})=(\hat{H}+\sigma\hat{I})^{-1}$, where σ is fixed at a value near the eigenvalues of interest.[61] The SI transform is not appropriate for our 2EFG method, however, since unlike the Fourier-grid representation of $\hat{H}$, $(\hat{H}+\sigma\hat{I})^{-1}$ has a dense matrix representation that cannot be compactly stored.

For our 2EFG method, we have therefore chosen an exact Chebychev polynomial transform,[62] which is defined in the interval of unwanted eigenvalues, $[E_{\text{cutoff}},E_{\max})$:

$$\Theta(\hat{H})=\prod_{j=1}^{m}(\hat{H}-\mu_j\hat{I}), \tag{A4}$$

where m is the order of a Chebychev polynomial,[62] the roots of which are

$$\mu_j=\frac{(E_{\max}+E_{\text{cutoff}})}{2}+\frac{(E_{\max}-E_{\text{cutoff}})}{2}\cos(\pi(2j-1)/2m). \tag{A5}$$

Use of the transform in Eq. (A4) amounts to simply applying the Hamiltonian matrix m times per IRLM iteration and therefore requires no additional storage. The choice of the parameters m,E_{cutoff}, and $E_{\max}$ is problem specific, however, and may involve some experimenting to find the optimal values. We found that a good strategy was to set E_{cutoff} 1.0 eV higher than the highest eigenvalue of interest (which in a MQC MD scheme can be evaluated from the previous time step). We also found that $E_{\max}$ is well approximated by the highest eigenvalue of the kinetic energy operator, $T_{\max}$, plus a first-order perturbation theory correction involving the potential energy. This makes sense since the high-energy part of the spectrum is dominated by the kinetic energy operator:

$$E_{\max}=T_{\max}+V_{\max}+r_{12\ \max}^{-1}, \tag{A6}$$

where

$$T_{\max}=2\times(2\pi/L)^2\frac{k_{\max}^2}{2}, \tag{A7}$$

$$V_{\max}=2\times\langle\boldsymbol{k}_{\max}|\hat{V}|\boldsymbol{k}_{\max}\rangle, \tag{A8}$$

and

$$r_{12\ \max}^{-1}=\langle\boldsymbol{k}_{\max}\boldsymbol{k}_{\max}|\hat{r}_{12}^{-1}|\boldsymbol{k}_{\max}\boldsymbol{k}_{\max}\rangle. \tag{A9}$$

In Eqs. (A6)–(A9), $\boldsymbol{k}_{\max}$ is the largest possible single-electron k-vector in the grid-based wave function expansion. Since $T_{\max}$ and $r_{12\ \max}^{-1}$ depend only on the size of the basis expansion and the length of the simulation cell, these parameters need to be calculated only once at the beginning of a simulation. In principle $V_{\max}$ is also constant throughout a MQC simulation because matrix elements involving plane waves are translationally invariant; however, since the potential energy operator is evaluated on a real-space grid, $V_{\max}$ does change slightly from time step to time step as particles move relative to the grid points. We therefore evaluate $V_{\max}$ every time the potential changes (i.e., at every MD time step in a MQC simulation) which amounts to taking a simple spatial average of $V(\boldsymbol{r})$ on the real-space grid, so that the actual Chebychev transform we apply varies slightly from simulation time step to simulation time step.

With the particular implementation of the Chebychev polynomial spectral transform discussed above, per IRLM

TABLE III. CPU time to calculate the lowest eigenvalue of sodide in THF with a Chebychev polynomial spectral transform (number of grid points, $N=16$. Further simulation details are described in Paper II, Sec. II. Timings are for a Dual Quad-Core 2.3 GHz Opteron processor).

m [a]	Time (s)[b]	#MV[c]
0	86.2	69.8
2	39.6	52
3	26.1	42
4	22.2	40
5	27.4	50
6	31.3	60

[a]m is the order of the Chebychev polynomial.
[b]Time to solve the TISE for the lowest state, averaged over 10 simulation time steps.
[c]#MV is the average number of Hamiltonian matrix-vector multiplications per time step.

iteration, the Hamiltonian matrix is applied m times more often than when diagonalizing the untransformed Hamiltonian matrix, where m is the chosen order of the polynomial. There is thus a trade-off between reducing the number of IRLM iterations by increasing m and reducing the number of Hamiltonian matrix-vector products per IRLM iteration by keeping m small. This balance is illustrated in Table III, which shows the diagonalization time and total number of Hamiltonian matrix-vector products to find the lowest electronic eigenstate of the two valence electrons of a sodium anion in THF (the condensed-phase system that is the subject of Paper II), averaged over 10 MD time steps. At each time step, the Lanczos diagonalization algorithm was initiated from the converged wave function at the previous time step. From this table we see that the diagonalization time is largely controlled by the total number of matrix-vector products and that both of these quantities have a minimum at $m=4$ for this particular system. Table III also highlights the effectiveness of the Chebychev polynomial spectral transform: there is roughly a factor of four speed-up in calculating the ground state of the transformed Hamiltonian ($m=4$) compared to the untransformed Hamiltonian ($m=0$). Use of the Chebychev polynomial transform becomes even more important when considering excited states, which often have near-degeneracies in the Hamiltonian's untransformed spectrum that would otherwise cause slow convergence in the Lanczos algorithm.[32]

[1] F. Webster, P. J. Rossky, and R. A. Friesner, Comput. Phys. Commun. **63**, 494 (1991).
[2] W. S. Sheu and P. J. Rossky, J. Phys. Chem. **100**, 1295 (1996).
[3] C. J. Smallwood, W. B. Bosma, R. E. Larsen, and B. J. Schwartz, J. Chem. Phys. **119**, 11263 (2003).
[4] V. S. Batista and D. F. Coker, J. Chem. Phys. **105**, 4033 (1996).
[5] G. H. Peslherbe, B. M. Ladanyi, and J. T. Hynes, J. Phys. Chem. A **102**, 4100 (1998).
[6] M. Persico, G. Granucci, S. Inglese, T. Laino, and A. Toniolo, J. Mol. Struct.: THEOCHEM **621**, 119 (2003).
[7] F. Sterpone and P. J. Rossky, J. Phys. Chem. B **112**, 4983 (2008).
[8] C. J. Smallwood, R. E. Larsen, W. J. Glover, and B. J. Schwartz, J. Chem. Phys. **125**, 074102 (2006).
[9] C. J. Smallwood, C. M. Mejia, W. J. Glover, R. E. Larsen, and B. J. Schwartz, J. Chem. Phys. **125**, 074103 (2006).
[10] R. E. Larsen and B. J. Schwartz, J. Chem. Phys. **119**, 7672 (2003).
[11] W. J. Glover, R. E. Larsen, and B. J. Schwartz, J. Chem. Phys. **129**, 164505 (2008).
[12] W. J. Glover, R. E. Larsen, and B. J. Schwartz, J. Phys. Chem. Lett. **1**, 165 (2010).
[13] W. J. Glover, R. E. Larsen, and B. J. Schwartz, J. Chem. Phys. **132**, 144102 (2010).
[14] E. R. Barthel, I. Martini, and B. J. Schwartz, J. Chem. Phys. **112**, 9433 (2000).
[15] I. B. Martini, E. R. Barthel, and B. J. Schwartz, J. Chem. Phys. **113**, 11245 (2000).
[16] E. R. Barthel, I. Martini, and B. J. Schwartz, J. Phys. Chem. B **105**, 12230 (2001).
[17] I. B. Martini, E. R. Barthel, and B. J. Schwartz, J. Am. Chem. Soc. **124**, 7622 (2002).
[18] E. R. Barthel and B. J. Schwartz, Chem. Phys. Lett. **375**, 435 (2003).
[19] E. R. Barthel, I. B. Martini, E. Keszei, and B. J. Schwartz, in *Ultrafast Phenomena XIII*, edited by M. Murnane, N. Scherer, R. J. D. Miller, and A. M. Weiner (Springer-Verlag, Berlin, 2003), pp. 459–461.
[20] I. B. Martini, E. R. Barthel, and B. J. Schwartz, in *Ultrafast Phenomena XIII*, edited by M. Murnane, N. Scherer, R. J. D. Miller, and A. M. Weiner (Springer-Verlag, Berlin, 2003), pp. 487–489.
[21] I. B. Martini and B. J. Schwartz, J. Chem. Phys. **121**, 374 (2004).
[22] I. B. Martini, E. R. Barthel, and B. J. Schwartz, Pure Appl. Chem. **76**, 1809 (2004).
[23] M. C. Cavanagh, R. E. Larsen, and B. J. Schwartz, J. Phys. Chem. A **111**, 5144 (2007).
[24] Z. H. Wang, O. Shoshana, B. X. Hou, and S. Ruhman, J. Phys. Chem. A **107**, 3009 (2003).
[25] O. Shoshana, J. L. P. Lustres, N. P. Ernsting, and S. Ruhman, Phys. Chem. Chem. Phys. **8**, 2599 (2006).
[26] O. Shoshanim and S. Ruhman, J. Chem. Phys. **129**, 044502 (2008).
[27] J. Jortner, M. Ottolenghi, and G. Stein, J. Phys. Chem. **68**, 247 (1964).
[28] Y. Gauduel, H. Gelabert, and M. Ashokkumar, Chem. Phys. **197**, 167 (1995).
[29] J. A. Kloepfer, V. H. Vilchiz, V. A. Lenchenkov, and S. E. Bradforth, Chem. Phys. Lett. **298**, 120 (1998).
[30] X. Chen and S. E. Bradforth, Annu. Rev. Phys. Chem. **59**, 203 (2008).
[31] See supplementary material at http://dx.doi.org/10.1063/1.3352564 for a discussion of how our 2EFG improves upon the real-space CISD method of Ref. 10.
[32] J. Collum and R. A. Wilboughby, *Lanczos Algorithms for Large Symmetric Eigenvalue Computations, Vol. 1, Theory* (Birkhäuser, Boston, 1985).
[33] A. Szabo and N. S. Ostlund, *Modern Quantum Chemistry* (Dover, Mineola, 1996).
[34] A. Alavi, J. Chem. Phys. **113**, 7735 (2000).
[35] R. E. Larsen and B. J. Schwartz, J. Phys. Chem. B **110**, 1006 (2006).
[36] R. E. Larsen and B. J. Schwartz, J. Phys. Chem. B **110**, 9681 (2006).
[37] R. E. Larsen and B. J. Schwartz, J. Phys. Chem. B **110**, 9692 (2006).
[38] P. Pulay, in *Applications of Electronic Structure Theory*, edited by H. F. Schaefer III (Plenum, New York, 1977).
[39] Y. Kubota and K. Nobusada, Comput. Phys. Commun. **177**, 43 (2007).
[40] Y. Kubota and K. Nobusada, Phys. Lett. A **369**, 128 (2007).
[41] R. Kosloff, J. Phys. Chem. **92**, 2087 (1988).
[42] E. Gabriel, G. E. Fagg, G. Bosilca, T. Angskun, J. J. Dongarra, J. M. Squyres, V. Sahay, P. Kambadur, B. Barrett, A. Lumsdaine, R. H. Castain, D. J. Daniel, R. L. Graham, and T. S. Woodall, Proceedings of the 11th European PVM/MPI Users' Group Meeting, Budapest, Hungary, 2004 (unpublished), pp. 97–104.
[43] D. C. Sorensen, SIAM J. Matrix Anal. Appl. **13**, 357 (1992).
[44] K. Maschhoff and D. Sorensen, *Proceedings of the Third International Workshop, PARA '96*, Lyngby, Denmark, 18–21 August 1996, edited by J. Wasniewski, J. Dongarra, K. Madsen, and D. Olesen (Springer-Verlag, Berlin, 1996), pp. 478–486.
[45] If $|\Psi\rangle$ is not in a pure spin state the identity in equation 10 will not hold; however, we enforce that $|\Psi\rangle$ be pure singlet or triplet throughout the calculation.
[46] P. M. Laufer and J. B. Krieger, Phys. Rev. A **33**, 1480 (1986).
[47] C. J. Huang and C. J. Umrigar, Phys. Rev. A **56**, 290 (1997).
[48] S. Ivanov, B. Burke, and M. Levy, J. Chem. Phys. **110**, 10262 (1999).
[49] S. Kais, D. R. Herschbach, N. C. Handy, C. W. Murray, and G. J. Laming, J. Chem. Phys. **99**, 417 (1993).
[50] C. Filippi, C. J. Umrigar, and M. Taut, J. Chem. Phys. **100**, 1290 (1994).
[51] M. Taut, A. Ernst, and H. Eschrig, J. Phys. B **31**, 2689 (1998).
[52] N. Rohringer, S. Peter, and J. Burgdorfer, Phys. Rev. A **74**, 042512 (2006).
[53] W. M. Zhu and S. B. Trickey, J. Chem. Phys. **125**, 094317 (2006).

[54] M. Taut, Phys. Rev. A **48**, 3561 (1993).
[55] J. Cioslowski and K. Pernal, J. Chem. Phys. **113**, 8434 (2000).
[56] W. Müller and W. Meyer, J. Chem. Phys. **80**, 3311 (1984).
[57] R. F. Barrow, J. Verges, C. Effantin, K. Hussein, and J. d'Incan, Chem. Phys. Lett. **104**, 179 (1984).
[58] L. Li, S. F. Rice, and R. W. Field, J. Chem. Phys. **82**, 1178 (1985).
[59] S. Magnier, P. Millié, O. Dulieu, and F. Masnou-Seeuws, J. Chem. Phys. **98**, 7113 (1993).
[60] Z. Liu, L. E. Carter, and E. A. Carter, J. Phys. Chem. **99**, 4355 (1995).
[61] Y. Saad, *Numerical Methods for Large Eigenvalue Problems* (Halsted Press, New York, 1992), Chap. 8.
[62] P. Pendergast, Z. Darakjian, E. F. Hayes, and D. C. Sorensen, J. Comput. Phys. **113**, 201 (1994).
[63] G. Gerber and R. Möller, Chem. Phys. Lett. **113**, 546 (1985).